Aerosol Remote Sensing over Clouds Using A-Train Observations

F. WAQUET, J. RIEDI, L. C. LABONNOTE, AND P. GOLOUB

Laboratoire d'Optique Atmosphérique, Université des Sciences et Technologies de Lille, Villeneuve-d'Ascq, France

B. CAIRNS

NASA Goddard Institute for Space Studies, New York, New York

J.-L. DEUZÉ AND D. TANRÉ

Laboratoire d'Optique Atmosphérique, Université des Sciences et Technologies de Lille, Villeneuve-d'Ascq, France

(Manuscript received 3 December 2008, in final form 2 March 2009)

ABSTRACT

The detection of aerosol above clouds is critical for the estimate of both the aerosol and cloud radiative impacts. In this study, the authors present a new method to retrieve the aerosol properties over clouds that uses the multiangle polarization measurements of the Polarization and Directionality of Earth Reflectances (POLDER)–Polarization and Anisotropy of Reflectances for Atmospheric Sciences Coupled with Observations from a Lidar (PARASOL) instrument. The method is illustrated and applied to a case study exploiting the coincident observations from other passive and active sensors of the NASA A-Train satellite constellation. The case study is relative to an elevated biomass burning aerosol layer that originates from southern Africa and is then transported over low-level clouds extending over the Atlantic Ocean. It is shown that the comparison between the cloud-top heights retrieved with the different passive techniques developed for the A-Train sensors can be used to detect the presence of aerosols above clouds. The analysis of the PARASOL observations showed that the aerosols significantly affect the polarized light reflected by the clouds over the 80°–120° scattering angle range and in the rainbow region. A single scattering model permitted the reproduction of the polarization observations and the retrieval of an estimate of the aerosol layer optical thickness of 0.225 at 0.865 μm. The retrieved aerosol optical thicknesses over clouds agree quantitatively with the closest ones retrieved over clear-sky ocean (± 0.04 as a maximum departure), demonstrating the value of the method. This innovative technique based solely on passive measurements is expected to provide a better understanding of aerosol properties in regions where significant cloud cover usually prevents the retrieval of aerosol optical thickness. As such, this new retrieval method can provide significant and valuable information about the radiative impact of clouds and aerosols, especially where they can potentially interact strongly with each other.

1. Introduction

Aerosol particles affect the climate of the earth directly by scattering and absorbing solar radiation and indirectly by affecting cloud microphysical properties (Bréon et al. 2002) and cloud lifetime. Although their net radiative effect may compensate for increases in the effects of greenhouse gases, the current magnitude and even the regional sign of their net effect remains uncertain (Forster et al. 2007). The constellation of National Aeronautics and Space Administration (NASA) satellites called the A-Train includes passive and active sensors specifically dedicated to the study of aerosol and cloud properties from a three-dimensional perspective, exploiting simultaneous and collocated multisensor observations (Stephens et al. 2002). Among these instruments, the Moderate Resolution Imaging Spectroradiometer (MODIS) and the Polarization and Anisotropy of Reflectances for Atmospheric Sciences Coupled with Observations from a Lidar (PARASOL) instrument take advantage respectively of multispectral measurements (0.41–14.2 μm) and spectral (0.44–0.865 μm) multidirectional and polarized passive measurements to

Corresponding author address: Dr. Fabien Waquet, LOA, UFR de Physique, Bât P5, USTL, Villeneuve-d'Ascq, CEDEX F-59655, France.
E-mail: waquet@loa.univ-lille1.fr

DOI: 10.1175/2009JAS3026.1

derive aerosol and cloud parameters on a global scale. The main aerosol parameters currently estimated from these measurements are the aerosol optical thickness (AOT) over both ocean (Tanré et al. 1997; Herman et al. 2005) and land (Kaufman et al. 1997; Deuzé et al. 2001; Hsu et al. 2004) and the particle size over ocean. For clouds, the current passive retrieval techniques provide, among other parameters, the cloud optical thickness, the thermodynamic phase (i.e., liquid or ice), the cloud particle size, and a number of different estimates of the cloud-top pressure (Parol et al. 1999; Platnick et al. 2003). Another interesting instrument is the Cloud–Aerosol Lidar with Orthogonal Polarization (CALIOP), which provides active measurements at 0.532 μm that are primarily used to determine the vertical structure of the atmosphere along the A-Train orbit track (Winker et al. 2004).

The determination of the atmospheric vertical structure, and particularly the organization of cloud and aerosol layers, is critical for the estimate of aerosol and cloud radiative impacts and for understanding their complex interactions. Biomass burning particles are usually injected into the atmosphere at high altitudes and can be transported over considerable distance and overlie low-level clouds (Cattani et al. 2006). Transport of mineral dust particles was also observed over clouds (De Graaf et al. 2007), although not so frequently. Recent studies have shown that the presence of aerosols above clouds affects the retrieval of cloud properties and the estimation of the indirect effect (Cattani et al. 2006). Biomass burning aerosols are usually strongly absorbing (Dubovik et al. 2002) and may therefore reduce the cloud albedo effect, causing a local positive radiative forcing. This latter process is not currently well understood and explains the large uncertainties associated with the estimation of the direct forcing by biomass burning particles (Forster et al. 2007).

Most of the current aerosol retrieval algorithms are restricted to cloud-free scenes, which strongly reduces our ability to monitor the aerosol properties at a global scale and thus limits the possibility of improving our knowledge of aerosol–cloud interactions. Active sensors constitute an obvious and well-defined observational approach to the detection of aerosols above bright clouds. However, current active sensors, and particularly the spaceborne instruments, have limited capabilities to accurately estimate the total aerosol burden without some available prior knowledge of the aerosol microphysics (Ackermann 1998; Cattrall et al. 2005); this is especially true during daytime because of increasing noise in the data (Kim et al. 2008). Furthermore, the better spatial coverage of passive sensors provides a clear advantage over active sensors in terms of sampling events when aerosol layers are above clouds, justifying the need for the development of passive remote sensing techniques that can provide qualitative (detection) and quantitative information about aerosol properties over cloud layers. A method based on the use of passive measurements acquired in a broad spectral range (0.28–1.75 μm) by the Scanning Imaging Absorption Spectrometer for Atmospheric Chartography (SCIAMACHY) instrument has been recently developed and allows us to detect UV-absorbing aerosols in cloud-contaminated scenes (De Graaf et al. 2007). The proposed method allows us to detect the absorbing particles using an aerosol index and provides an estimate of aerosol optical thickness and single scattering albedo, under some assumptions made about aerosol and cloud microphysical properties. In this study, we describe an original method of aerosol characterization over clouds, based on the use of A-train observations. The technique used to detect the presence of aerosols above the clouds relies on the comparison of cloud-top heights retrieved with the different passive techniques developed for the A-train sensors. The aerosol retrieval algorithm is solely based on the use of multiangle polarization measurements in the visible and near-infrared wavelengths from the Polarization and Directionality of Earth Reflectances (POLDER)–PARASOL instruments. The proposed algorithm allows retrieving the aerosol optical thickness and a parameter indicative of particle size. Furthermore, this algorithm has the advantage of being only weakly sensitive to the microphysical properties of the clouds located below the aerosol layer. This innovative method is illustrated and applied to a case study exploiting the coincident observations from other passive and active sensors of the A-Train satellite constellation. In the next section, we present a case study of a layer of particles from biomass burning observed over low-level clouds and the A-Train observations allowing its detection. The third section is dedicated to the interpretation of the polarized observations and presents a simple method used to retrieve the AOT. The fourth section presents some examples of aerosol retrievals performed above clouds. The last section summarizes the results and concludes by discussing the interesting perspectives opened by this innovative technique for the study of cloud and aerosol interactions.

2. Analysis of an aerosol transport case study

An episode of biomass burning aerosol transport from southwest Africa to the Atlantic Ocean was analyzed using simultaneous and collocated POLDER–PARASOL, MODIS, and CALIOP observations. The analysis of the case study, conducted during 14–18 August 2006, allowed

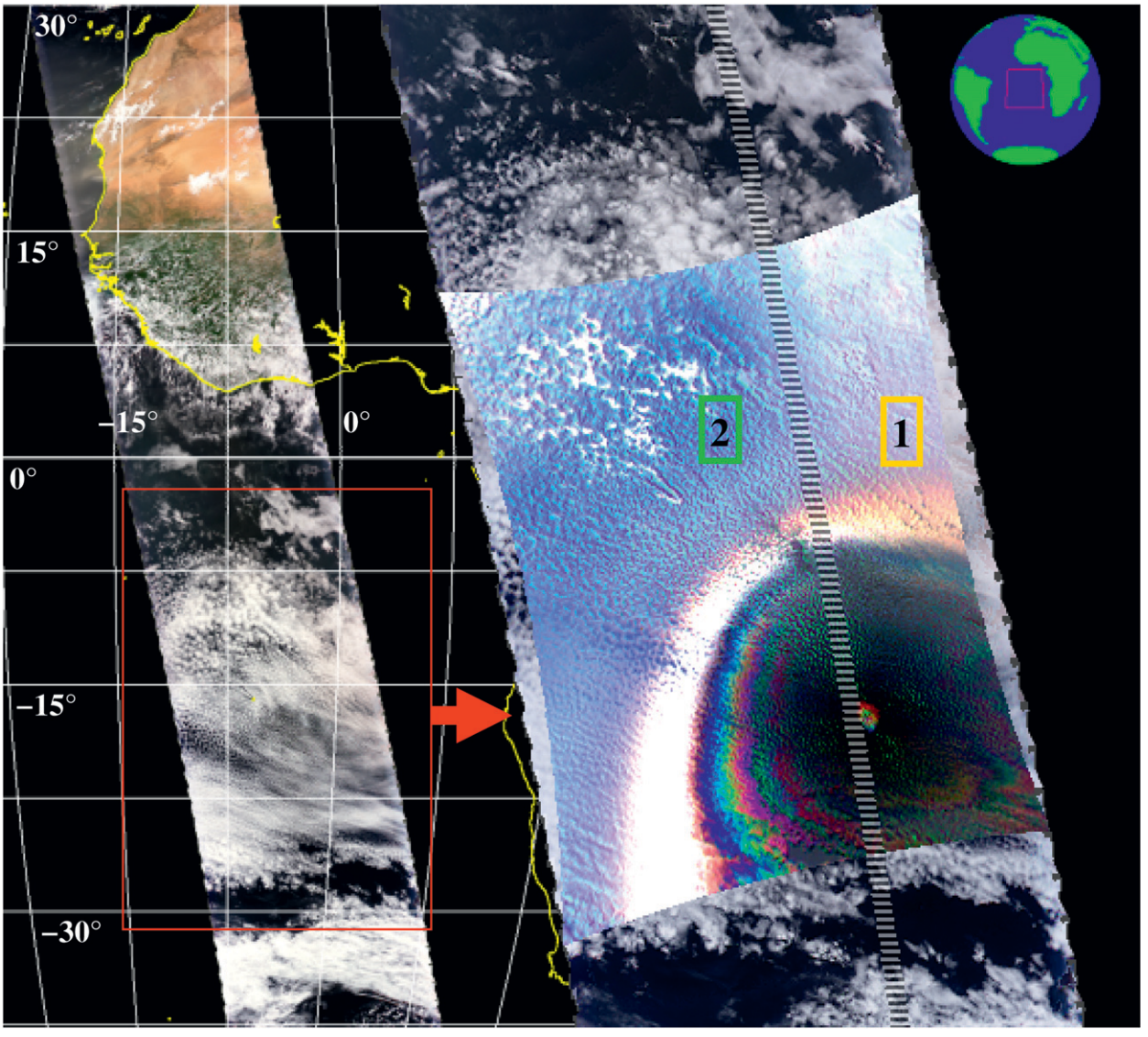

FIG. 1. Red–green–blue (RGB) composites relative to 1400 UTC 18 Aug 2006 POLDER/PARASOL measurements in (left) total radiance and (right) polarized radiance for the area in the red box. The dashed line on the right RGB composite represents the CALIOP orbit track. The yellow and green boxes correspond respectively to areas with and without aerosol above the clouds. On the RGB composite with polarized radiances, note the primary rainbow feature, typically observed in presence of water clouds, which is darkened in the upper east part of the image because of the presence of aerosol above the cloud top.

us to identify a methodology for detecting the presence of an aerosol layer above cloud top and estimating the corresponding AOT value. The quantities used to derive the aerosol and cloud properties from POLDER are the total and polarized normalized radiance (unitless) as defined in Herman et al. (2005). Throughout the rest of the paper, when we discuss radiances, we will be referring to these normalized quantities. Figure 1 (left) is a true color composite image illustrating PARASOL total radiance observations on 18 August 2006 over western Africa and the Atlantic Ocean. The red box delimits the cloudy area investigated in the paper. Figure 1 (right) is a false color composite image combining polarized radiances at 0.490, 0.670, and 0.865 μm for the selected area. The CALIOP orbit track is illustrated in Fig. 1 (right) and the corresponding atmospheric vertical features derived from CALIOP observations are shown in Fig. 2 along with the different coincident POLDER and MODIS retrievals of cloud-top pressure. The aerosol and cloud layers shown in Fig. 2 can be discriminated from each other based on the amplitude and spectral behavior of the lidar signal measured in two

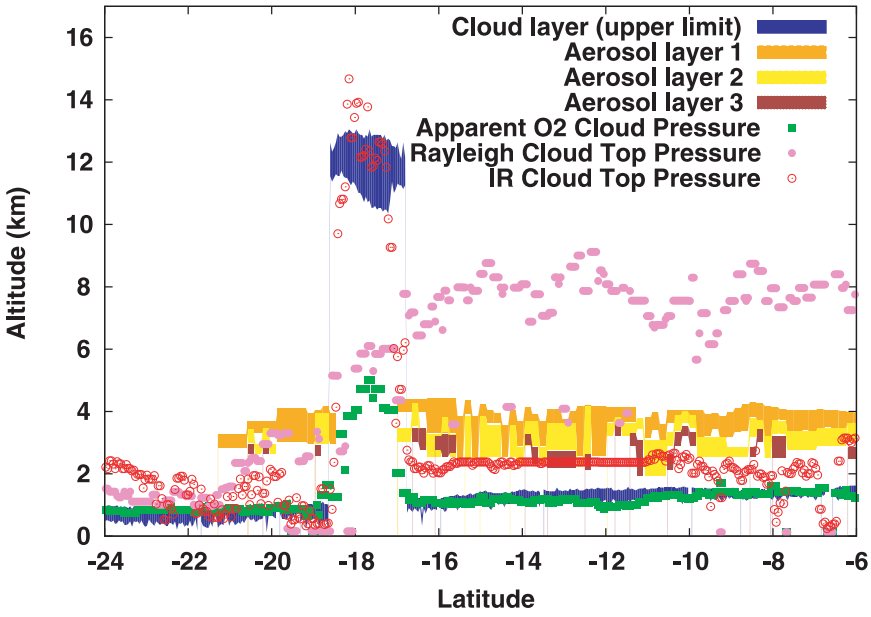

FIG. 2. Cloud and aerosol layer structures derived from the CALIOP measurements as a function of latitude (solid lines). Cloud-top heights are retrieved using different passive remote sensing techniques (dots). The corresponding CALIOP orbit track is shown in Fig. 1.

spectral bands and using an adaptive threshold technique (Vaughan et al. 2004). The CALIOP atmospheric features correspond to a product at 5-km resolution (CLAY5KM and ALAY5KM; Vaughan et al. 2004). The MODIS cloud pressure has been extracted from the MOD06 cloud product, which provides data at a resolution of 5 km × 5 km (Platnick et al. 2003); the POLDER data correspond to the radiative budget level 2 (RB2) cloud products given at a pixel resolution of 18.5 km × 18.5 km (Parol et al. 2004). For the comparison shown in Fig. 2, we selected the POLDER and MODIS pixels whose centers are the closest to those of the CALIOP pixels.

Figure 2 shows an aerosol layer located between 2 and 4 km above low-level clouds with cloud-top heights varying between 0.7 and 1.3 km. A cirrus cloud is observed between latitudes −16.5° and −19.5° above the low cloud layer. The heights of the low-level cloud base are not derived by CALIOP, which indicates that the measurements were acquired under thick cloud conditions (Kim et al. 2008). The origin of the aerosols observed between 2 and 4 km was inferred using back trajectories from the National Oceanic and Atmospheric Administration (NOAA) Hybrid Single-Particle Lagrangian Integrated Trajectory (HYSPLIT) model and the AOT retrieved by PARASOL. The aerosol layer originated from the biomass fires that occur annually in southern Africa between August and September (Tanré et al. 2001). Biomass burning particles mainly contribute to the AOT of the aerosol fine mode, which is associated with particles smaller than 0.6 μm in size (Dubovik et al. 2002). During the 14–18 August time period, the largest fine-mode AOTs (>0.3 at 0.865 μm) were observed in western Congo and north of Angola (see Fig. 6a for latitude >−14° and longitude <20°). The biomass burning particles were transported over the course of three or four days over the African continent and then over the Atlantic Ocean (see Fig. 6a), prior to their detection above the clouds on 18 August. The back trajectories also suggest that the biomass burning particles were located within the boundary layer in the source regions (altitudes <1.5 km) and were rapidly lifted over the African continent and then transported at an almost constant altitude.

The presence of the aerosol layer above the clouds was initially detected by its perturbing effects on the cloud-top pressure estimated from passive observations. We reported in Fig. 2 the uppermost cloud-top height, z_c, determined from CALIOP, along with altitude derived from (i) the "Rayleigh cloud-top pressure" method (z_c_Rayleigh), which is based on the use of spectral polarized radiance measurements (Goloub et al. 1994); (ii) the "apparent O_2 cloud pressure" method (z_c_O_2), which uses differential absorption measurements in the oxygen A-band (Vanbauce et al. 2003); and (iii) the "IR cloud-top pressure" method (z_c_IR), which uses MODIS measurements acquired in the thermal infrared (Menzel et al. 2006). Figure 2 shows for latitudes lower than 22°, where no aerosol layers over clouds were detected, the

differences between these methods typically observed in the case of a single low-level cloud. We usually observe small departures that are due to the respective sensitivity of each method to cloud-top height (i.e., z_c_IR > z_c_Rayleigh > z_c_O_2). The differences are expected to increase in the case of multiple cloud layers, as shown between latitudes −16.5° and −19.5°. In the case of aerosols above clouds, we observe a nontypical behavior (z_c_Rayleigh ≫ z_c_IR > z_c_O_2) as the cloud-top height estimated with the "Rayleigh" method is significantly larger than the ones derived with the two other techniques. The comparison between the CALIOP observations and the cloud-top height passive retrievals clearly shows that the Rayleigh technique is affected by the presence of aerosols above the clouds. It also shows that the "O_2" technique is not strongly perturbed and still allows the cloud-top height to be estimated with an accuracy of ±350 m, at least for this case study. We also compared the cloud-top heights retrieved with the different passive techniques for the entire cloudy area selected in Fig. 1. We observed anomalies in the cloud-top heights due to aerosols (z_c_Rayleigh ≫ z_c_IR > z_c_O_2), such as the ones observed along the CALIOP track or even larger, in the western part of the cloudy areas, and to a lesser extent, over their northern and northeastern parts. As shown later (see Fig. 6b), these areas correspond to regions where our algorithm retrieves significant loads of aerosols above the clouds (AOT > 0.15 at 0.87 μm). This confirms that the comparison of the different cloud-top heights can be used to detect the presence of aerosols above the clouds without using an elaborate retrieval approach.

The presence of aerosols above the clouds can be also detected by using only the polarized radiance measurements. Figure 1 (right) shows the primary rainbow, which corresponds to an intense polarized signal that appears almost spectrally neutral (white circular structure). This is a feature typically observed in polarization for liquid clouds at a scattering angle of around 140° from the incident direct solar beam (Goloub et al. 2000). Figure 1 (right) shows that the primary rainbow is darkened and turns brown in the upper east part of the image because of the presence of aerosols above the clouds. This is explained by the fact that aerosols attenuate the signal reflected by cloud in the rainbow region. Because the observed particles are associated with a spectrally dependent AOT (i.e., fine-mode particles), they affect the rainbow differently as a function of the wavelength. To further investigate the effects of aerosols above clouds on the polarized radiance measurements, we segregated PARASOL measurements into two small boxes of about 200 km per 100 km and made use of the multiangular capabilities of PARASOL for each box. Box 1 corresponds to an area where aerosols were detected above the clouds (i.e., z_c_Rayleigh ≫ z_c_IR > z_c_O_2), whereas box 2 corresponds to an unpolluted cloudy area. Figure 3 shows the polarized radiances measured by PARASOL at 865 nm for each box in Fig. 1 (right) as a function of the scattering angle. The curve in Fig. 3a (blue symbols) shows the angular polarized signature typically observed for water clouds, which is characterized by a strong maximum around 140° (primary rainbow) and small polarized reflectance values over the 90°–120° range (Goloub et al. 2000). The curve in Fig. 3b (red symbols) highlights an abnormal angular polarized signature for a water cloud, with larger polarized reflectance values over the 90°–120° range and smaller polarized reflectance values in the primary rainbow peak. The additional polarization signal corresponds to the polarized radiance generated by aerosols located above the clouds.

3. Retrieval method: Modeling and inversion

Single scattering approximations have been commonly used to model the polarized light reflected by the atmosphere–surface system of the earth (Bréon and Goloub 1998; Deuzé et al. 2001). Following these previous studies, we model the polarized radiance emerging from a plane-parallel system constituted by an atmosphere above a thick cloud (cloud optical thickness >5) by considering only the single scattering by molecules and aerosols and only one interaction between atmosphere and cloud. The polarized radiance Lp_λ emerging from such a system can be written as

$$Lp_\lambda(\theta_s, \theta_v, \varphi_r) = \frac{q^m(\Theta)\tau_\lambda^m}{4\mu_v} + \frac{\omega_{0,\lambda}^a q_\lambda^a(\Theta)\tau_\lambda^a}{4\mu_v} \exp(-m\gamma\tau_\lambda^m) + Lp_\lambda^c(\theta_s, \theta_v, \varphi_r) \exp[-m(\gamma\tau_\lambda^m + \beta\tau_\lambda^a)], \quad (1)$$

where μ_s and μ_v are the cosines of the solar zenith angle θ_s and the view zenith angle θ_v, respectively; φ_r is the relative azimuth angle, m is the so-called "air mass" factor ($m = \mu_s^{-1} + \mu_v^{-1}$), and Θ is the scattering angle. Also, λ denotes a quantity that depends on the wavelength, and q^m is the polarized phase function for molecules that includes the effects of the depolarization of air:

$$q^m(\Theta) = 0.96\frac{3}{4}(1 - \cos^2\Theta), \quad (2)$$

where τ_λ^m is the molecular optical thickness above the cloud, which is given by

$$\tau_\lambda^m = \tau_\lambda^{m\_\mathrm{tot}} \exp\left(-\frac{z_c}{8}\right), \quad (3)$$

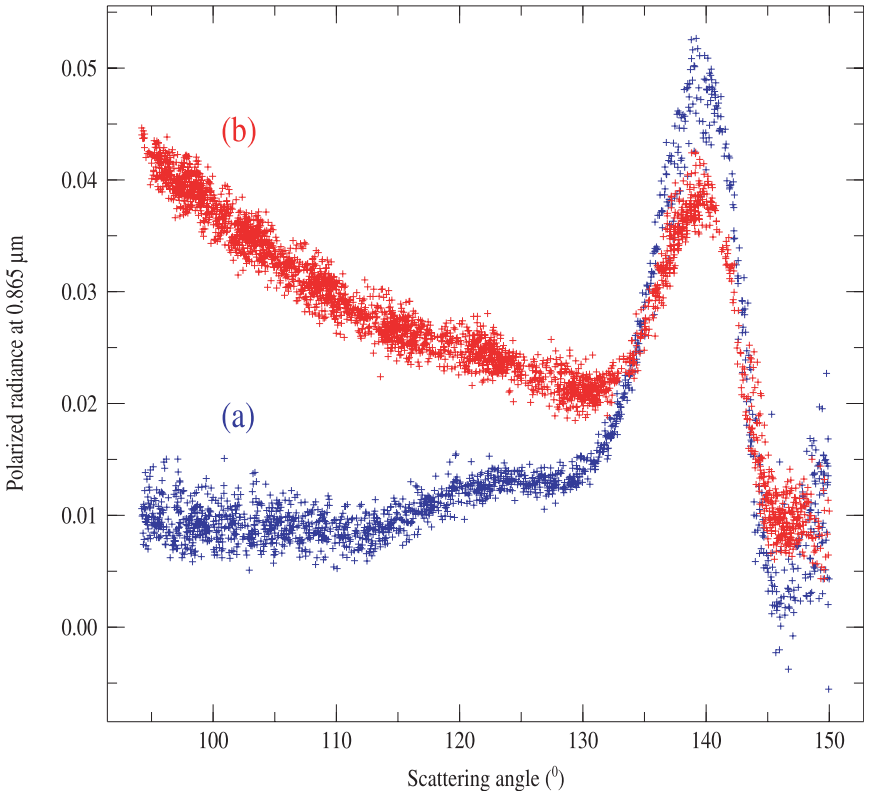

FIG. 3. Polarized radiances measured by PARASOL at 0.865 μm as a function of the scattering angle for the two boxes shown in Fig. 1 (right): (a) blue symbols represent the radiances relative to box 2, where only low clouds are present; (b) red symbols represent the data of box 1, where a significant load of biomass burning was detected above the clouds.

where $\tau_\lambda^{m\_\mathrm{tot}}$ is the total molecular optical thickness at λ (Hansen and Travis 1974), τ_λ^a is the optical thickness of the aerosol above the cloud, and $\omega_{0,\lambda}^a$ and q_λ^a are respectively the aerosol single scattering albedo and the aerosol polarized phase function (i.e., the F12 component of the scattering phase matrix). The aerosol optical properties are calculated using Mie theory. Also, $L_{p\lambda}^c$ is the polarized radiance reflected by the cloud; the γ and β coefficients account for diffuse transmission of light by aerosols and molecules, which reduces their screening effect on the radiation (Bréon et al. 1995). These coefficients are empirically derived following Lafrance (1997); γ is equal to 0.9 and β varies between 0.3 and 0.6 depending on the aerosol model.

Figure 4 shows polarized radiances calculated at 0.67 μm with an adding/doubling radiative transfer code (De Haan et al. 1987) and those computed with Eq. (1) for an atmosphere constituted by a thick liquid cloud with and without aerosols above the cloud. The adding/doubling radiative transfer code allows the multiple scattering properties of any atmosphere to be calculated. The atmosphere is described as a juxtaposition of infinite plane-parallel layers, each layer being defined by the vertical distribution of scatterers and their scattering properties. The scattering properties and vertical distribution of Rayleigh scattering are defined as in Eqs. (2) and (3). The clouds and aerosols particles are homogeneously distributed respectively throughout the first lowest kilometer of the atmosphere and between 1 and 3 km. The scattering properties of the clouds and aerosols particles are calculated using the Mie theory. The liquid water droplet model consists of a gamma size distribution (Deirmendjian 1969), with an effective radius of 10.0 μm and effective variance of 0.1. The aerosol model consists of spherical small particles described by a single lognormal size distribution with effective radius of 0.149 μm and effective variance of 0.175. The complex refractive index of the aerosol is fixed to 1.47–0.01i. The simulations confirm the polarized features observed by PARASOL in the case of cloudy scenes polluted by a fine aerosol mode (i.e., attenuated cloud bow and large L_p values over the 80°–120° range). Fine-mode particles typically show large polarized phase function values for scattering angles between 80° and 120° (see Fig. 1 in Waquet et al. 2007). This feature explains why the polarized radiance

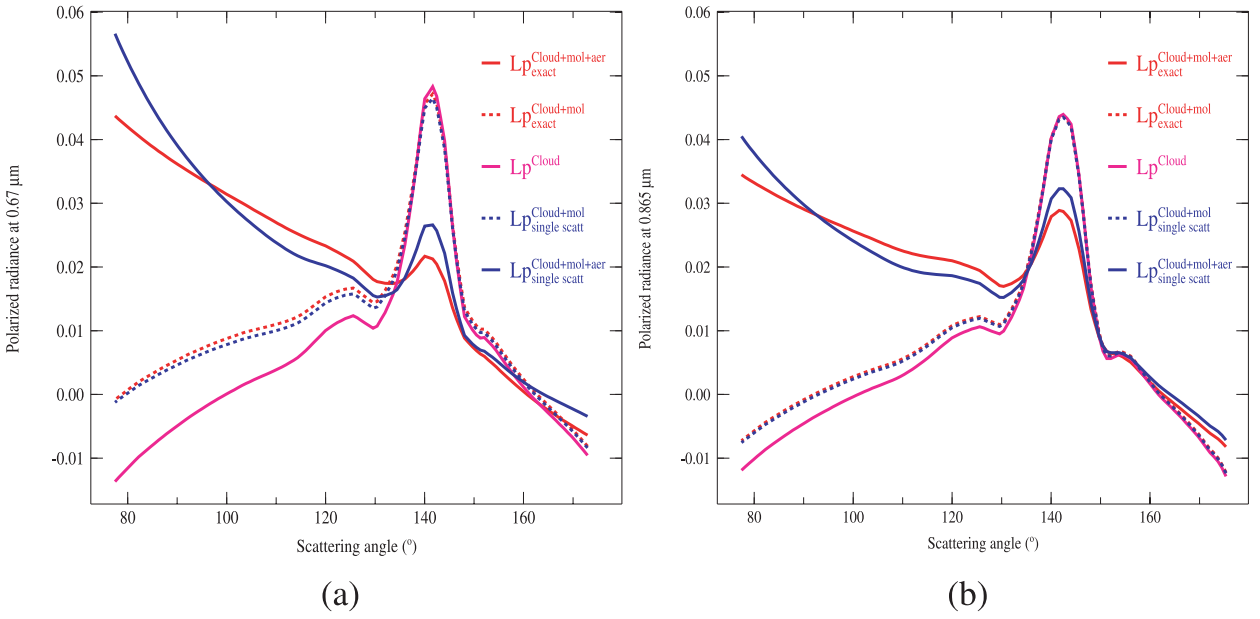

FIG. 4. (a) Polarized radiances simulated at 0.67 μm with the adding/doubling radiative transfer code by De Haan et al. (1987) for an atmosphere composed of a thick liquid cloud with an aerosol layer above the cloud top (solid red line), without the aerosol (dashed red line), and for the cloud alone (magenta line) as a function of the scattering angle. Blue curves represent the polarized radiances computed with Eq. (1) (single-scattering approximation) for the liquid cloud with (solid blue line) and without the aerosol layer (dashed blue line). (b) As in (a), but for calculations made at 0.865 μm. In both (a) and (b), $\theta_s = 50°$, $\varphi_s - \varphi_v = 0°$, $\tau_a = 0.5$ at 0.67 μm, $r_{\text{eff}} = 0.149$ μm, $v_{\text{eff}} = 0.1735$, $m_r = 1.47–0.01i$, $r^c_{\text{eff}} = 10$ μm, and $v^c_{\text{eff}} = 0.1$, for a cloud extended between 0 and 1 km.

at side scattering angles increases as the aerosol optical thickness increases [see the second term of Eq. (1)]. In the rainbow region, aerosol particles polarize much less than cloud particles. Therefore, the aerosol layer primarily attenuates the clouds' contribution to the polarized signal in this region [see the third term of Eq. (1)]. Moreover, the cloud bow's attenuation depends on molecules and aerosol amount above the cloud, and so it is stronger as the wavelength decreases. This explains why the cloud bow appears much more attenuated in Fig. 4a than in Fig. 4b (see red solid lines); the aerosol optical thickness for a fine-mode aerosol is significantly larger at 0.67 μm than at 0.87 μm. Our simple model provides a reasonable fit to the reference model calculations. However, in the case of aerosols above the cloud (AOT of 0.5 at 0.670 μm), the model significantly overestimates the signal at lower scattering angles ($<90°$) and in the primary rainbow region ($\approx 140°$) and underestimates the signal over the 110°–130° range. Additional calculations show that these errors are mainly due to inaccurate modeling of the diffuse interactions between the cloud and the free atmosphere (Waquet et al. 2009). The presence of aerosols above the clouds is primarily responsible for the increase in the diffuse cloud–atmosphere interactions. In case of aerosols above the clouds, there is a larger amount of diffuse light that reaches the clouds because aerosols have larger forward scattering properties than molecules. The polarized light reflected by the cloud is preferentially scattered by the aerosols in the forward scattering direction, which also tends to increase the contribution of diffuse cloud–atmosphere interactions to the radiation field emerging at TOA. The importance of such processes increases with decreasing wavelength; for this reason, the retrieval method described here is limited to the use of the polarized radiances measured at 0.670 and 0.865 μm.

Simulations show that the polarized radiance reflected by a cloud is saturated for cloud optical thickness larger than 3 (Goloub et al. 2000). This means that the quantity $L^c_{p\lambda}$ in Eq. (1) only depends on the cloud droplet effective radius and variance as long as the cloud is thick enough for the polarization signal to saturate. The sensitivity of $L^c_{p\lambda}$ to the cloud droplet effective radius is rather small for scattering angles lower than 130° whereas the sensitivity to the effective variance only appears for angles larger than 145° (see Figs. 1 and 2 in Goloub et al. 2000). In our retrieval approach, this quantity is precomputed for a set of viewing geometries (θ_s, θ_v, φ_r) using a multiple scattering code (Deuzé et al. 1989) and is interpolated to the sensor viewing geometry. We consider several cloud droplet size distributions (Bréon and Goloub 1998), described by 16 droplet effective radii varying between 5 and 20 μm and an effective variance of 0.1. We select the cloud

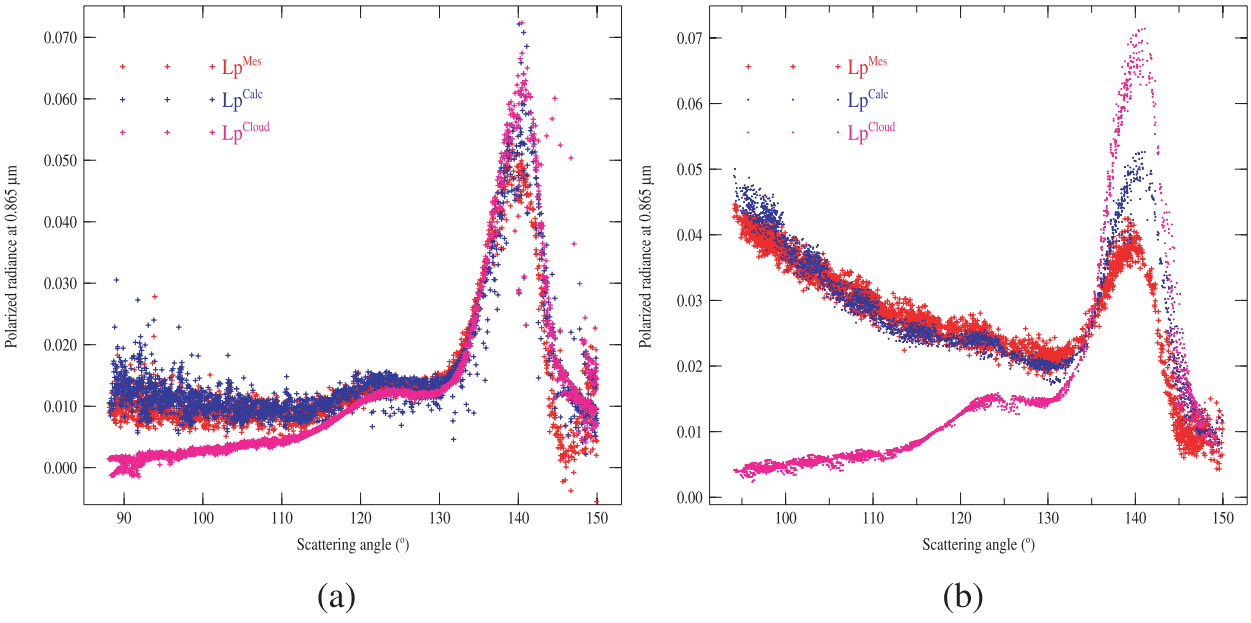

FIG. 5. (a) Polarized radiances measured by PARASOL at 0.865 μm (red) for box 2, saturated polarized radiances for a liquid cloud calculated using the microphysical properties retrieved by MODIS (magenta), and polarized radiances fitted with our algorithm (blue). (b) As in (a), but for box 1.

droplet effective radius based on the collocated simultaneous MODIS effective radius retrieval (Platnick et al. 2003). Polarized radiances measurements at 0.67 and 0.865 μm are primarily sensitive to the properties of the fine-mode particles (Waquet et al. 2007). We therefore consider 15 aerosol models in the algorithm, which consists of a single lognormal size distribution of small spherical particles with an effective radius varying between 0.089 and 0.54 μm and an effective variance of 0.173. We assume that the refractive index is 1.47–0.01i, which is the mean value for fine-mode particles (Dubovik et al. 2002). The cloud-top altitude in Eq. (3) is estimated using the O_2 method, which was shown to be accurate along the CALIOP satellite track (Fig. 2), and we assume that the O_2 method is accurate over the entire selected cloudy scene. This assumption is supported by the fact that the cloud properties retrieved by MODIS along the CALIOP orbit track are consistent with those retrieved over the full area (i.e., optically thick low-level liquid clouds), which means that the O_2 technique should provide the cloud-top height with a comparable accuracy to that shown in Fig. 2. The polarized radiances are calculated with Eq. (1) for each aerosol model and for aerosol optical thicknesses increasing by steps of 0.001 between 0.0 and 1.5 at 865 nm. The aerosol model and aerosol optical thickness that minimize a least squares error term calculated between the simulated and measured polarized radiances at 0.670 and 0.865 μm (Deuzé et al. 2001) define our retrieved quantities.

Figures 5a and 5b show an example of fitting obtained from our method applied to the 0.865-μm POLDER polarized radiances of boxes 2 and 1 (see Fig. 1), respectively. Red symbols represent the measured polarized radiances, blue symbols represent the simulated polarized radiances that fit the measured data, and the polarized radiances of the cloud alone calculated using the MODIS cloud effective radius values are in magenta. These results show that our model reproduces the measured polarized radiances at 0.865 μm, except in the rainbow region and for scattering angles larger than 145°. The departures observed between the measured and the fitted polarized radiances are larger at 0.670 μm but do not exceed those predicted by the simulations (see Fig. 4). To provide the best possible AOT estimates, we restrict our algorithm to the 90°–110° scattering angle range because over this range (i) the aerosol contribution is maximal, (ii) the method is only weakly sensitive to the cloud microphysical properties and the effects of potential biases in the retrieved cloud droplet effective radii are minimized, and (iii) the modeling errors introduced by Eq. (1) are minimized. We also used a cloud screening criteria to ensure that our analysis was only applied to cloudy pixels associated with an overcast cloud cover and a high cloud optical thickness (to ensure that the polarization cloud signal is saturated). The cloud screen took advantage of the high spatial resolution retrieval capabilities of MODIS (1×1 km^2 at nadir) to estimate within each PARASOL pixel (6×6 km^2) a mean value and a

standard deviation for both the cloud optical thickness and the cloud droplet effective radius. In the analysis presented here, we only keep the PARASOL pixels associated with a mean cloud optical thickness larger than 5, a cloud optical thickness standard deviation smaller than 4, and a cloud droplet effective radius standard deviation smaller than 2.

4. Results

Figure 6a shows the fine-mode AOTs retrieved by PARASOL at 0.865 μm over the Atlantic Ocean and southern Africa for cloud-free pixels. Figure 6b shows the AOTs retrieved over cloud and over ocean with a higher-resolution ''zoom'' view of the selected cloudy area. The AOTs retrieved by PARASOL over land and ocean are operationally provided at a resolution of 18×18 km^2. We therefore average our retrievals to match that resolution. We calculate a mean AOT when a minimum of five subpixels are available and we only keep the AOT value when the associated standard deviation is smaller than 0.05. These two criteria only weakly reduce the number of observations but they do allow us to eliminate some obviously dubious retrievals at cloud edges. The comparison between Figs. 6a and 6b allows us to distinguish the retrievals made over the cloudy and cloud-free areas. We observe good coherence between the retrievals performed over ocean, land, and clouds. The strongest AOTs are retrieved in the eastern part of the cloudy area, which is the closest one to the source region. The ocean–cloud AOT transitions observed at the northern and southern edges of the cloudy area are qualitatively good. The spatial heterogeneity of the retrievals over clouds is satisfying, especially over the thickest and the most homogeneous cloudy areas (e.g., for $-25° <$ latitude $< -20°$ and $-10° <$ longitude $< -4°$). The biomass burning aerosol layer observed in the eastern part of cloudy area is associated with a mean AOT of 0.225 at 0.865 μm and an aerosol model effective radius equal to 0.15 μm. The order of magnitude of the smoke plume AOT is coherent with other passive retrievals made over ocean. It is also very consistent with retrievals on the previous day (17 August 2006), when PARASOL observed fine-mode AOTs ranging between 0.18 and 0.24 at 0.865 μm between the selected cloudy area and the African coasts ($-10° <$ latitude $< -5°$ and $5° <$ longitude $< 10°$). We also compare our retrievals with the MODIS ones acquired over ocean on 18 August 2006. The ocean–cloud AOT transitions observed in the region of the smoke plume are small, on the order of about 0.04, with the MODIS retrievals being systematically slightly larger than our retrievals. This comparison is presented only as an indication of qualitative agreement since the aerosol properties that were retrieved by MODIS are on the edge of the cloudy area and may therefore be cloud contaminated (Kaufman et al. 2005). These discrepancies may also result from differences in the aerosol models used in the respective algorithm. We also considered the ultraviolet Aerosol Index (AI) provided by the Ozone Monitoring Instrument (OMI) for the comparison. The AI is sensitive to ultraviolet-absorbing particles such as smoke particles and allows their detection in cloud-free and cloud-contaminated scenes over both ocean and land. This quantity increases with the aerosol optical thickness in the UV but also depends on the absorption and altitude of the aerosols (Herman et al. 1997). OMI uses two spectral bands centered on 0.331 and 0.360 μm to derive the AI at a resolution (at nadir) of 13 km $\times$ 24 km (Ahmad et al. 2006) and provides measurements only 6 min after POLDER. The spatial distribution of the AI agrees qualitatively with our AOT estimates made over clouds (not shown). The largest AI values are notably observed where our algorithm retrieves the largest AOT values (e.g., $2.0 <$ AI < 3.5 for $-19° <$ latitudes $< -11°$ and $-2° <$ longitudes $< 4°$). OMI also systematically shows low AI values (<1.0) when our algorithm retrieves small AOTs over the clouds (<0.06 at 0.865 μm).

We finally apply the method to another case of biomass burning particles overlying clouds, detected during the same event but observed closer to the source regions. The northwestern part of southern Africa was partially covered by low thick liquid clouds at the time of the A-train overpass on 18 August 2006. The comparison between the cloud-top heights retrieved with the different passive techniques showed that a significant amount of smoke was transported over this area. Figure 7a shows the fine-mode AOT at 0.865 μm retrieved by POLDER on 18 August 2006 over southern Africa for the cloud-free pixels. Figure 7b shows the same quantity retrieved for both cloud-free and cloudy pixels. The spatial distribution of the AOT retrieved above the clouds again agrees qualitatively well with the spatial distribution of the AOT retrieved over cloud-free regions. We can notably observe a progressive decrease in the AOT retrieved above the clouds in the northwestern part of the image as we move away from the fire regions. The maximal AOT values are retrieved in the vicinity of the source regions and are larger than in the previous example (>0.3 at 0.865 μm), as expected. The retrieved aerosol model is the same as the one previously retrieved for most of the observations (80% for AOT > 0.1 at 0.865 μm). This additional example confirms that our method is quite insensitive to the variability in cloud properties and also that it is stable with respect to particle size retrieval, at least for this specific biomass burning event.

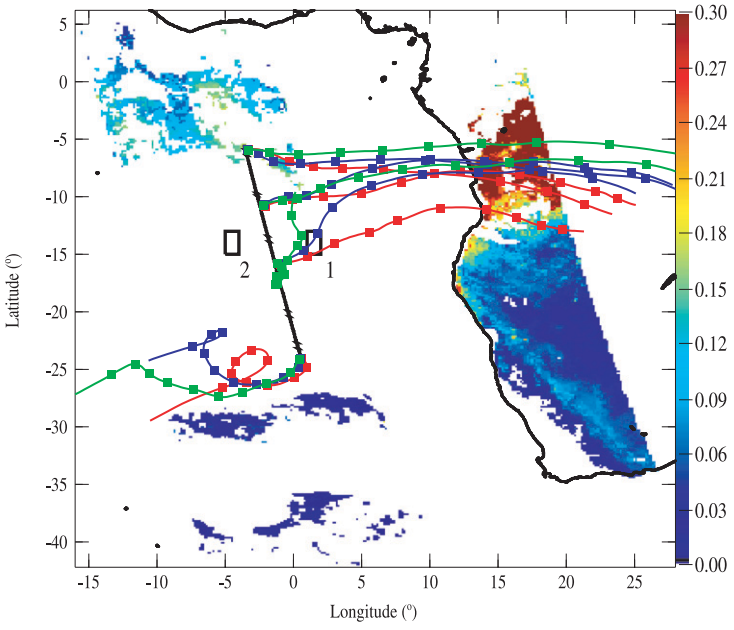

(a)

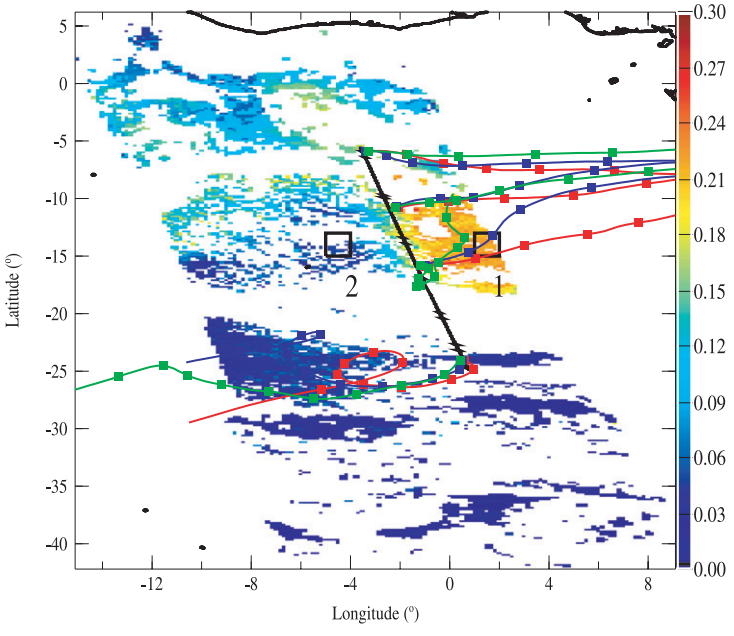

(b)

FIG. 6. (a) Fine-mode aerosol optical thickness retrieved at 0.865 μm by PARASOL over ocean and land cloud-free pixels. The back trajectories (solid lines) of the air masses calculated for altitudes equal to 2, 3, and 4 km are in red, green, and blue, respectively. The squares denote calculations separated from 12 h. The straight black solid line corresponds to the CALIOP track segment shown in Fig. 2. The ending points of the back trajectories are located on the CALIOP track segment (see Fig. 2 for longitudes equal to −6°, −11°, −15°, and −24°). (b) In the zoomed area, AOT values for cloudy scenes are reported in addition to the AOT values for clear pixels. Land AOT values are relative to the PARASOL overpass of 1200 UTC 14 Aug, whereas AOT values over ocean refer to 1400 UTC 18 Aug.

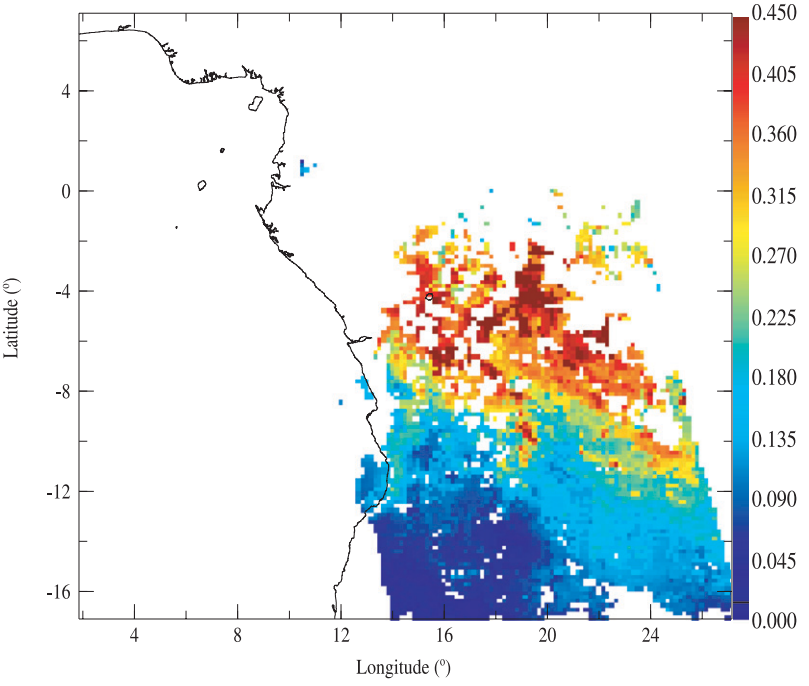

(a)

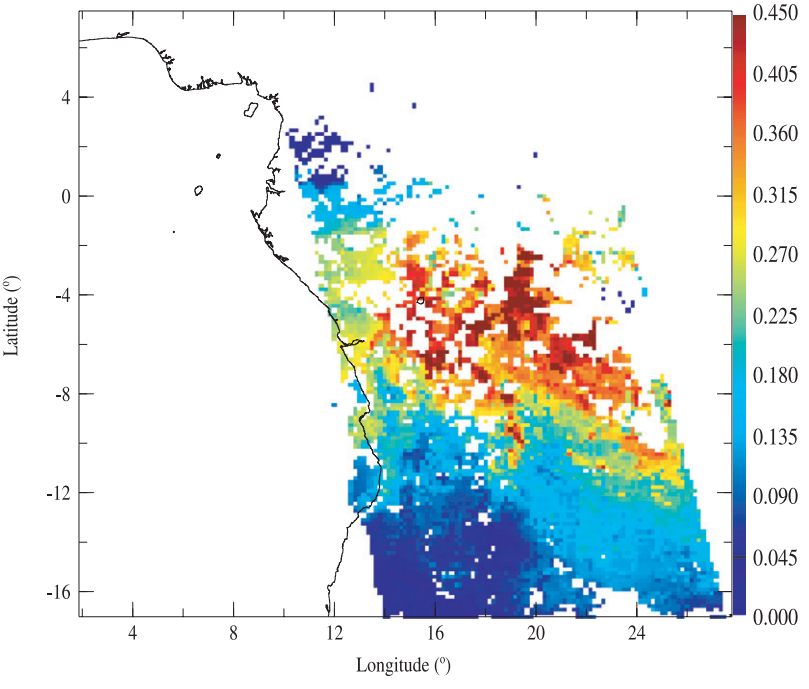

(b)

FIG. 7. (a) Fine-mode aerosol optical thickness retrieved at 0.865 μm by PARASOL over ocean and land cloud-free pixels. (b) As in (a), but with AOT values for cloudy scenes. The AOT values are relative to the PARASOL overpass of 1400 UTC 18 Aug.

5. Conclusions

We described A-Train observations that allowed the detection of an African biomass-burning aerosol layer transported above low-level clouds extending over the Atlantic Ocean. The comparison between the cloud-top heights retrieved with the different passive techniques developed for the A-Train sensors can be used to detect the presence of aerosols above clouds. This is an important result because it means that A-Train observations can be used to identify polluted cloudy areas where the current passive techniques developed for cloud study either should not be used or should at least be identified as being potentially impacted by aerosol contamination. The analysis of the PARASOL observations and the use of simulations showed that aerosols significantly affect the polarized light reflected by the clouds in the rainbow region and over the 80°–120° scattering angle range. These polarized features together with the fact that the O_2 technique allows the cloud-top height to be estimated make it possible to retrieve the aerosols properties above low-level clouds using a simple approach. A single scattering model of the free atmosphere allowed us to reproduce the polarized observations reasonably well and to retrieve an estimate of the aerosol layer AOT of about 0.225 at 0.865 μm. The AOTs retrieved over clouds agree quantitatively with the closest ones retrieved over clear-sky ocean ($\pm$0.04 as a maximum departure), demonstrating the value of our method. This innovative technique will allow aerosol information to be derived operationally over stratocumulus clouds in the near future from POLDER. This is expected to provide a better understanding of aerosol properties in regions where significant cloud cover usually prevents the retrieval of aerosol optical thickness. Also, this will help us understand the radiative interactions between aerosols and cloud layers in regions where clouds have a strong radiative forcing. Finally, this new technique opens interesting prospects for the use of next-generation polarimeters. For instance, the present technique could benefit from the inclusion of the highly accurate, multiangle, multispectral (0.41–2.25 μm) polarized measurements provided by the future Aerosol Polarimeter Sensor (APS), which will join the A-train in 2010. The adding of polarization measurements at shorter visible wavelengths would provide better sensitivity to aerosol microphysics (Chowdhary et al. 2002; Waquet et al. 2009), whereas the high-angular measurements resolution of APS could be used to accurately estimate the clouds droplet size distribution using polarization observations at large scattering angles (Bréon and Goloub 1998). The next step is to improve the method used for the multiple scattering computations and to evaluate the possibility of including the retrieval of cloud properties in the inversion. This, of course, is constrained mostly by the computational cost of full radiative transfer simulations and the availability of practical inversion techniques. The future applications of this work are the estimation of the occurrence of aerosol transport over clouds, their impact on cloud property retrievals, and their radiative impacts on a global scale using the 3 yr of observations made by the A-Train.

Acknowledgments. The authors are very grateful to CNES and NASA for providing the POLDER, MODIS, and CALIOP data used in this study. We thank the ICARE Data and Services Center for providing access to the data and for general assistance and development support. Thanks are also due to Francois Thieuleux and Fabrice Ducos for support with data processing and analysis. This research has been supported by CNES, CNRS, the University of Lille, and Region Nord-Pas-de-Calais.

REFERENCES

Ackermann, J., 1998: The extinction-to-backscatter ratio of tropospheric aerosol: A numerical study. *J. Atmos. Oceanic Technol.,* **15,** 1043–1050.

Ahmad, S. P., O. Torres, P. K. Bhartia, G. Leptoukh, and S. Kempler, 2006: Aerosol index from TOMS and OMI measurements. Preprints, *14th Joint Conf. on the Applications of Air Pollution Meteorology,* Atlanta, GA, Amer. Meteor. Soc., P1.6. [Available online at http://ams.confex.com/ams/pdfpapers/104496.pdf.]

Bréon, F.-M., and P. Goloub, 1998: Cloud droplet effective radius from spaceborne polarization measurements. *Geophys. Res. Lett.,* **25,** 1879–1882.

——, D. Tanré, P. Leconte, and M. Herman, 1995: Polarized reflectance of bare soils and vegetation: Measurements and models. *IEEE Trans. Geosci. Remote Sens.,* **33,** 487–499.

——, ——, and S. Generoso, 2002: Aerosol effect on cloud droplet size monitored from satellite. *Science,* **295,** 834–838.

Cattani, E., M. J. Costa, F. Torricella, V. Levizzani, and A. M. Silva, 2006: Influence of aerosol particles from biomass burning on cloud microphysical properties and radiative forcing. *Atmos. Res.,* **82,** 310–327, doi:10.1016/j.atmosres.2005.10.010.

Cattrall, C., J. Reagan, K. Thome, and O. Dubovik, 2005: Variability of aerosol and spectral lidar and backscatter and extinction ratios of key aerosol types derived from selected Aerosol Robotic Network locations. *J. Geophys. Res.,* **110,** D10S11, doi:10.1029/2004JD005124.

Chowdhary, J., B. Cairns, and L. Travis, 2002: Case studies of aerosol retrievals from multiangle, multispectral photopolarimetric remote sensing data. *J. Atmos. Sci.,* **59,** 383–397.

De Graaf, M., P. Stammes, and E. A. A. Aben, 2007: Analysis of reflectance spectra of UV-absorbing aerosol scenes measured by SCIAMACHY. *J. Geophys. Res.,* **112,** D02206, doi:10.1029/2006JD007249.

De Haan, J. F., P. B. Bosma, and J. W. Hovenier, 1987: The adding method for multiple scattering calculations of polarized light. *Astron. Astrophys.,* **183,** 371–391.

Deirmendjian, D., 1969: *Electromagnetic Scattering on Spherical Polydispersions*. Elsevier, 318 pp.

Deuzé, J.-L., M. Herman, and R. Santer, 1989: Fourier series expansion of the transfer equation in the atmosphere–ocean system. *J. Quant. Spectrosc. Radiat. Transfer,* **41,** 483–494.

——, and Coauthors, 2001: Remote sensing of aerosols over land surfaces from POLDER-ADEOS-1 polarized measurements. *J. Geophys. Res.,* **106,** 4913–4926.

Dubovik, O., B. Holben, T. F. Eck, A. Smirnov, Y. J. Kaufman, M. D. King, D. Tanré, and I. Slutsker, 2002: Variability of absorption and optical properties of key aerosol types observed in worldwide locations. *J. Atmos. Sci.,* **59,** 590–608.

Forster, P., and Coauthors, 2007: Changes in atmospheric constituents and in radiative forcing. *Climate Change 2007: The Physical Science Basis,* S. Solomon et al., Eds., Cambridge University Press, 129–234

Goloub, P., J. L. Deuzé, M. Herman, and Y. Fouquart, 1994: Analysis of the POLDER polarization measurements performed over cloud covers. *IEEE Trans. Geosci. Remote Sens.,* **32,** 78–88.

——, M. Herman, H. Chepfer, J. Riedi, G. Brogniez, P. Couvert, and G. Séze, 2000: Cloud thermodynamical phase classification from the POLDER spaceborne instrument. *J. Geophys. Res.,* **105,** 14 747–14 760.

Hansen, J. E., and L. D. Travis, 1974: Light scattering in planetary atmospheres. *Space Sci. Rev.,* **16,** 527–610.

Herman, J. R., P. Bhartia, O. Torres, C. Hsu, C. Seftor, and E. Celarier, 1997: Global distribution of UV-absorbing aerosol from Nimbus-7/TOMS data. *J. Geophys. Res.,* **102,** 16 911–16 922.

Herman, M., J.-L. Deuzé, A. Marchand, B. Roger, and P. Lallart, 2005: Aerosol remote sensing from POLDER/ADEOS over the ocean: Improved retrieval using a nonspherical particle model. *J. Geophys. Res.,* **110,** D10S02, doi:10.1029/2004JD004798.

Hsu, N. C., S. C. Tsay, M. D. King, and J. R. Herman, 2004: Aerosol retrievals over bright-reflecting source regions. *IEEE Trans. Geosci. Remote Sens.,* **42,** 557–569.

Kaufman, Y. J., D. Tanré, L. Remer, E. Vermote, A. Chu, and B. Holben, 1997: Operational remote sensing of tropospheric aerosol over land from EOS moderate resolution imaging spectroradiometer. *J. Geophys. Res.,* **102,** 17 051–17 067.

——, and Coauthors, 2005: A critical examination of the residual cloud contamination and diurnal sampling effects on MODIS estimates of aerosol over ocean. *IEEE Trans. Geosci. Remote Sens.,* **43,** 2886–2897.

Kim, S.-W., S. Berthier, J.-C. Raut, P. Chazette, F. Dulac, and S.-C. Yoon, 2008: Validation of aerosol and cloud layer structures from the space-borne lidar CALIOP using a ground-based lidar in Seoul, Korea. *Atmos. Chem. Phys.,* **8,** 3705–3720.

Lafrance, B., 1997: Modélisation simplifiée de la lumière polarisée émergeant de l'atmosphère: Correction de l'impact des aérosols stratosphériques sur les mesures de POLDER. Ph.D. thesis, Université des Sciences et Techniques de Lille, 114 pp.

Menzel, W. P., R. A. Frey, B. A. Baum, and H. Zhang, 2006: Cloud top properties and cloud phase algorithm theoretical basis document, version 7, 55 pp. [Available online at http://modis-atmos.gsfc.nasa.gov/_docs/MOD06CT:MYD06CT_ATBD_C005.pdf.]

Parol, F., J. C. Buriez, C. Vanbauce, P. Couvert, G. Sèze, P. Goloub, and S. Cheinet, 1999: First results of the POLDER "Earth Radiation Budget and Clouds" operational algorithm. *IEEE Trans. Geosci. Remote Sens.,* **37,** 1597–1612.

——, and Coauthors, 2004: Capabilities of Multi-Angle Polarization Cloud measurements from satellite: POLDER results. *Adv. Space Res.,* **33,** 1080–1088.

Platnick, S., M. D. King, S. A. Ackerman, W. P. Menzel, B. A. Baum, J. C. Riédi, and R. A. Frey, 2003: The MODIS cloud products: Algorithms and examples from *Terra*. *IEEE Trans. Geosci. Remote Sens.,* **41,** 459–473.

Stephens, G. L., and Coauthors, 2002: The CloudSat mission and the A-TRAIN: A new dimension of space-based observations of clouds and precipitation. *Bull. Amer. Meteor. Soc.,* **83,** 1771–1790.

Tanré, D., Y. J. Kaufman, and S. Mattoo, 1997: Remote sensing of aerosol properties over oceans using the MODIS/EOS spectral radiances. *J. Geophys. Res.,* **102,** 16 971–16 988.

——, F.-M. Bréon, J.-L. Deuzé, M. Herman, P. Goloub, F. Nadal, and A. Marchand, 2001: Global observation of anthropogenic aerosols from satellite. *Geophys. Res. Lett.,* **28,** 4555–4558.

Vanbauce, C., B. Cadet, and R. T. Marchand, 2003: Comparison of POLDER apparent and corrected oxygen pressure to ARM/MMCR cloud boundary pressures. *Geophys. Res. Lett.,* **30,** 1212, doi:10.1029/2002GL016449.

Vaughan, M., S. Young, D. Winker, K. Powell, A. Omar, Z. Liu, Y. Hu, and C. Hostetler, 2004: Fully automated analysis of space-based lidar data: An overview of the CALIPSO retrieval algorithms and data products. *Laser Radar Techniques for Atmospheric Sensing,* U. N. Singh, Ed., International Society for Optical Engineering (SPIE Proceedings, Vol. 5575), 16–30, doi:10.1117/12.572024.

Waquet, F., P. Goloub, J.-L. Deuzé, J. F. Léon, F. Auriol, C. Verwaerde, J.-Y. Balois, and P. François, 2007: Aerosol retrieval over land using a multiband polarimeter and comparison with path radiance method. *J. Geophys. Res.,* **112,** D11214, doi:10.1029/2006JD008029.

——, B. Cairns, K. Knobelspiesse, J. Chowdhary, L. D. Travis, B. Schmid, and M. I. Mishchenko, 2009: Polarimetric remote sensing of aerosols over land. *J. Geophys. Res.,* **114,** D01206, doi:10.1029/2008JD010619.

Winker, D. M., W. H. Hunt, and C. A. Hostetler, 2004: Status and performance of the CALIOP lidar. *Laser Radar Techniques for Atmospheric Sensing,* U. N. Singh, Ed., International Society for Optical Engineering (SPIE Proceedings, Vol. 5575), 8–15, doi:10.1117/12.571955.